



# Formation of the low-field peak in magnetization loops of high- $T_c$ superconductors

M.R. Koblishchka <sup>a,\*</sup>, L. Půst <sup>b,2</sup>, M. Jirsa <sup>b</sup>, T.H. Johansen <sup>a</sup>

<sup>a</sup> Department of Physics, University of Oslo, P.O. Box 1048, N-0316 Oslo, Norway

<sup>b</sup> Academy of Sciences of the Czech Republic, Institute of Physics, Na Slovance 2, CZ-18040 Praha 8, Czech Republic

Received 21 December 1998; received in revised form 19 April 1999; accepted 24 May 1999

---

## Abstract

The positions of the central (low-field) peak in the magnetization hysteresis loops (MHLs) are analyzed in various high- $T_c$  superconducting samples comprising several  $\text{RBa}_2\text{Cu}_3\text{O}_{7-\delta}$  (RBCO; R = rare earths) single crystals of different thicknesses, a laser-ablated  $\text{YBa}_2\text{Cu}_3\text{O}_{7-\delta}$  (YBCO) thin film, Ag-sheathed  $(\text{Pb,Bi})_2\text{Sr}_2\text{Ba}_2\text{Cu}_3\text{O}_{10+\delta}$  (Bi-2223) mono- and multifilamentary tapes, and a model sample designed to reproduce a layer of grains [M.R. Koblishchka et al., Appl. Phys. Lett. 70 (1997) 514]. The single crystals and the thin film show the peak at zero-field or at negative applied fields on the descending field branch according to the critical state models, the Bi-2223 tapes are found to exhibit the peak anomalously in positive applied fields. In order to better understand the magnetization processes leading to the formation of the central peak in the MHLs, the local field distributions in applied fields close to zero were studied using magneto-optic (MO) flux visualization on the same samples. These flux patterns show how the vortices are rearranged when sweeping through zero-field. A large demagnetizing effect (“perpendicular geometry”) facilitates the penetration of vortices of opposite polarity, especially along structural defects, thus, forcing the central peak towards zero or even to very small positive fields. To explain the anomalous behaviour found in Bi-2223 tapes, effects of granularity have to be considered additionally. Further, we discuss the interaction of the central peak with other “peak effects” observed in MHLs. © 1999 Published by Elsevier Science B.V. All rights reserved.

PACS: 74.60 Ec; 74.60 Ge; 74.60 Jg

Keywords: Magnetization hysteresis loops; Bi-2223; Perpendicular geometry; High- $T_c$  superconducting samples

---

## 1. Introduction

Observations of various ‘anomalous’ peaks on magnetization hysteresis loops (MHLs) in high- $T_c$  samples have revived the interest to study specific properties of magnetization processes in these novel materials. Up to now, three types of maxima have been observed, each with a distinct temperature behaviour: the central or low-field peak at fields close

---

\* Corresponding author. Fax: +81-3-3454-9284; E-mail: koblishchka@istec.or.jp

<sup>1</sup> Present address: ISTEC/Superconductivity Research Laboratory, 1-16-25, Shibaura, Minato-ku, Tokyo 105, Japan.

<sup>2</sup> Present address: Seagate Technology, Bloomington, MN 55435, USA.

to 0 T; the fishtail or secondary peak at relatively high fields (typically ranging between 1 and 5 T at 77 K), and sometimes even an intermediate peak between the central and the fishtail peak. Whereas the origin of the fishtail and intermediate peaks are widely discussed in literature [1–10], only little attention is paid to the properties of the low-field peak within a MHL [11–17]. In various experiments, however, it could be observed that the central peak is located at zero-field, or at small negative fields on the descending field branch depending on the aspect ratio of the sample  $r_0/d$ , where  $r_0$  denotes the diameter of the sample and  $2d$  is the thickness.

Very recently, MHLs of  $(\text{Pb,Bi})_2\text{Sr}_2\text{Ca}_2\text{Cu}_3\text{O}_{10+\delta}$  (Bi-2223) mono- and multifilamentary tapes showed another, rather unexpected feature: The central peak is here found at relatively large *positive* fields on the descending field branch [18–21]. However, it is evident that multifilamentary tapes exhibit the anomalous peak position much less pronounced [22].

All these observations made clear that a detailed study of magnetization processes in high- $T_c$  superconductors is required, as a number of properties may affect the shape of hysteresis loops, e.g., large internal anisotropy, layered structures, granularity, geometrical aspect ratio, temperature dependent effects, etc. Therefore, in this paper, we present a detailed investigation of the properties of the central peak for various high- $T_c$  superconductors. Furthermore, we combine the analysis of the MHL data with the observation of local field distributions obtained around 0 T using magneto-optic (MO) imaging [23] in order to achieve a better understanding of this field region. This technique enables us to study the behaviour of the internal field,  $B_i$ , for a given external field,  $B_e$ .

Assuming that the local current density decreases monotonously with increasing local field, a maximum on the MHL is expected at  $\langle B_i \rangle_m = 0$  where  $\langle B_i \rangle_m$  denotes an average of the local fields,  $B_i$ , weighted with respect to the individual contributions of the local critical currents to the total magnetic moment  $m$ . Taking into account a simple case of a dome-like flux distribution inside the sample (which is typical for the case of a long superconductor in a magnetic field parallel to the long axis, usually called ‘longitudinal geometry’),  $B_i$  lags behind the external field  $B_e$  in all the sample volume. In this

way, the position of the central peak  $B_{pc}$  has to be negative on the descending field branch and positive on the ascending field branch of the MHL [24,25]. In practice, in high- $T_c$  samples, we usually meet another situation of a flat sample of a strongly anisotropic material, being magnetized along its  $c$ -axis which is oriented normal to the sample plane (‘perpendicular geometry’). Demagnetizing effects play a significant role in this case. Theoretical treatments of this geometry are only available recently; and many aspects of the central peak are not yet clarified. Recently, in Ref. [26], it is shown that the position of the central peak in a thin strip is located *strictly at 0 T for any* field dependence of the current density,  $j_c(B)$ . Another result is that one more additional effect is sufficient to bring the peak position to the positive side. As we will see in the present paper, this can be due to granularity, the sample shape or even structural defects. To test our model presented in Ref. [21], we prepared a ‘‘model sample’’ from a thin film with artificially introduced granularity.

This paper is organized as follows. In Section 2, some details about the sample preparation and measurement techniques are given. Section 3.1 describes the results of the magnetic measurements. In Section 3.2, we present the local flux distributions of several high- $T_c$  samples. In Section 4, we discuss the process of formation of the central peak, peculiarities found in the flux patterns, and the possible influence of the central peak on the observation of other peak effects within a MHL. Finally, in Section 5, we summarize our results.

## 2. Experimental procedure

### 2.1. Sample preparation

Various high- $T_c$  samples were chosen for this study; among them, five  $\text{RBa}_2\text{Cu}_3\text{O}_{7-\delta}$  (RBCO; R = rare earths) single crystals of different thickness and microstructure, two  $\text{YBa}_2\text{Cu}_3\text{O}_{7-\delta}$  (YBCO) epitaxial thin films, and pieces of mono- and multifilamentary Bi-2223 tapes. Furthermore, a sample with artificially introduced granularity (‘‘model sample’’), prepared using a laser-ablated YBCO thin film, is also investigated.

Table 1  
Properties of the samples used in this study

Sample name	Type	Sample size	Remarks
Crystal A	$\text{DyBa}_2\text{Cu}_3\text{O}_{7-\delta}$	$1.2 \times 0.8 \times 0.015 \text{ mm}^3$	twinned
Crystal B	$\text{YBa}_2\text{Cu}_3\text{O}_{7-\delta}$	$1.0 \times 1.0 \times 0.08 \text{ mm}^3$	twinned
Crystal C	$\text{YBa}_2\text{Cu}_3\text{O}_{7-\delta}$	$1.1 \times 1.05 \times 0.3 \text{ mm}^3$	twinned
Crystal D	$\text{YBa}_2\text{Cu}_3\text{O}_{7-\delta}$	$1.1 \times 1.3 \times 1.05 \text{ mm}^3$	twinned
Crystal E	$\text{YBa}_2\text{Cu}_3\text{O}_{7-\delta}$	$2.3 \times 1.5 \times 0.2 \text{ mm}^3$	detwinned mechanically
Thin film	$\text{YBa}_2\text{Cu}_3\text{O}_{7-\delta}$	$1.4 \times 0.66 \text{ mm}^2$ , $d = 200 \text{ nm}$	free of structural defects, MO investigations, see Ref. [27]
“Model sample”	$\text{YBa}_2\text{Cu}_3\text{O}_{7-\delta}$	$1.2 \times 0.8 \text{ mm}^2$ , $d = 150 \text{ nm}$	$\approx 8000$ disks with $2r = 50 \mu\text{m}$ , see Refs. [28,29]
Monofilamentary tape	$(\text{Pb,Bi})_2\text{Sr}_2\text{Ca}_2\text{Cu}_3\text{O}_{10+\delta}$	$1.2 \times 0.8 \times 0.015 \text{ mm}^3$	MO investigations, see Refs. [30,31]
Multifilamentary tape	$(\text{Pb,Bi})_2\text{Sr}_2\text{Ca}_2\text{Cu}_3\text{O}_{10+\delta}$	$1.2 \times 0.8 \times 0.015 \text{ mm}^3$	19 filaments, MO investigations, see Refs. [22,30,31]

The properties of these samples are summarized in Table 1. The RBCO single crystals were grown by a self-flux method in  $\text{SnO}_2$  and Y-stabilized  $\text{ZrO}_2$  crucibles as described in Ref. [32]. The crystals C, D and E were also studied by MO imaging.

The YBCO films were prepared by laser ablation on a MgO substrate [33]. The thickness was 200 nm, and the samples were patterned by chemical etching into a rectangular shape of dimensions  $0.66 \times 1.4 \text{ mm}^2$ . MO imaging revealed that the samples contained a very small amount of structural defects; the sample chosen for the MO investigations and the magnetic measurements turned out to be completely free of defects [27]. Another YBCO thin film of the same batch with exactly one defect serves as an example to demonstrate how defects alter the flux patterns.

The Ag-sheathed Bi-2223 tapes were prepared by the standard ‘powder-in-tube’ method with subsequent, drawing and rolling [34], resulting in a tape with an overall width of 3 mm. The pieces cut for the investigation was 4 mm long. The superconducting core of the monofilamentary tape was about 15  $\mu\text{m}$  thick; the multifilamentary tape comprised of 19 filaments. A detailed MO analysis of flux patterns of these tapes can be found in Refs. [22,30,31,35].

The model sample was prepared by means of laser ablation on a  $\text{LaAlO}_3$  substrate. The thickness of the YBCO thin film was 150 nm. A structure of hexagonally close packed circular disks was then patterned by means of electron-beam lithography [28,29]. The diameter of the disks,  $2r$ , is 50  $\mu\text{m}$ . and

the contact width,  $w = 3.5 \mu\text{m}$ . The sample had an overall size of  $4 \times 4 \text{ mm}^2$ , comprising  $\approx 8000$  disks. The transition temperature,  $T_c$ , after the patterning process was about 83 K.

## 2.2. Magnetic measurements

The magnetization measurements were performed using two magnetometers: (i) a vibrating sample magnetometer (VSM) PAR Model 155 with computer control and data processing. The magnetic field is generated by a conventional magnet with  $B_{e,\text{max}} \pm 2 \text{ T}$  and (ii) a Quantum Design MPMS 5 SQUID magnetometer with a superconducting solenoid ( $B_{e,\text{max}} \pm 5 \text{ T}$ ). In both magnetometers, the field is applied parallel to the  $c$ -axis (perpendicular to the sample plane).

## 2.3. MO imaging

The MO visualization techniques are described in detail in Ref. [23], so a short summary suffices here. The field distribution is visualized by means of the Faraday effect, i.e., the rotation of the polarization plane of linearly polarized light which passes a magneto-optically active layer exposed to the magnetic field of the underlying superconductor. From flux-free regions, the light is reflected without rotation and thus cannot pass the analyzer which is set in a crossed position with respect to the polarizer. In this way, areas penetrated by flux are imaged as bright areas (the brightness is, therefore, a measure

of the vortex density), whereas the flux-free Meissner areas stay dark. As a result, the images presented here are maps of the  $z$ -component of the local magnetic field,  $B_z$ . As a magneto-optically active layer a Bi-doped yttrium–iron–garnet film with in-plane anisotropy was used. The thickness of the active layer was  $4 \mu\text{m}$ , half of which corresponds to the spatial resolution of our experiment. The images were recorded using an 8 bit Kodak DCS 420 CCD digital camera ( $1536 \times 1024$  pixels per frame) and subsequently transferred to a computer for processing and storage. In the MO apparatus, the sample was mounted on the cold finger of a helium gas-flow optical cryostat [23,36]. The magnetic field was applied along the plane normal to the sample surface using a copper solenoid with a maximum field of  $\pm 120$  mT.

### 3. Experimental results

#### 3.1. Magnetization measurements

The magnetization loops were measured always after zero-field cooling the sample. All RBCO single

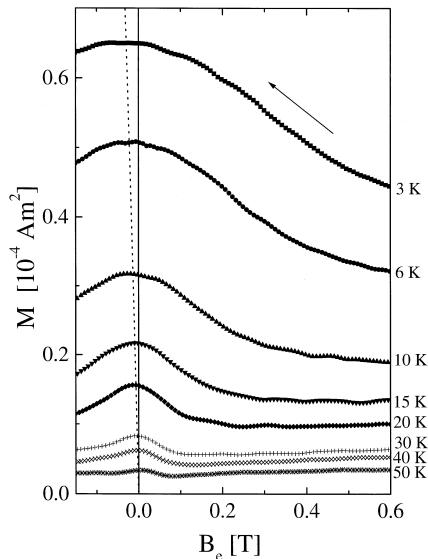


Fig. 1. Magnetization loops of a DyBCO single crystal (sample A, thickness of  $15 \mu\text{m}$ ) at temperatures of 3, 6, 10, 15, 20, 30, 40, and 50 K. The figure shows that at the lowest temperatures the central peak is located at slightly negative applied fields ( $B_{\text{pc}} = -0.035$  T at  $T = 3$  K). The arrows indicate the direction of the field sweep.

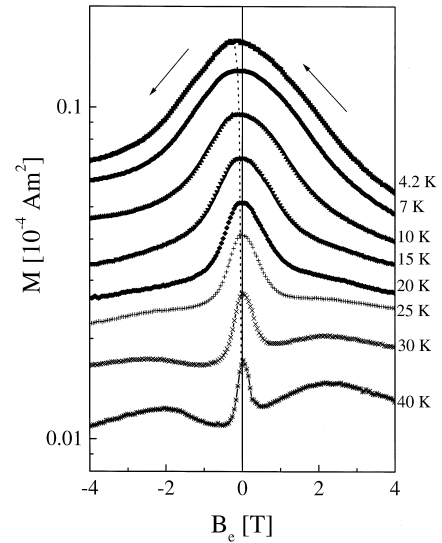


Fig. 2. Temperature dependence of the central peak in a MHL, measured on sample B with a thickness of  $80 \mu\text{m}$ . The temperatures are  $T = 4.2, 7, 10, 15, 20, 25, 30,$  and  $40$  K (from top to bottom). The dashed line indicates the temperature behaviour of the central peak. The arrows indicate the direction of the field sweep.

crystals investigated here exhibit the fishtail effect, so also the interplay between the central peak and the fishtail peak can be analyzed.

In Fig. 1, the decreasing field branch MHLs measured on sample A are presented at temperatures of 3, 6, 10, 15, 20, 30, 40, and 50 K. Fig. 1 shows that at the lowest temperatures the central peak is located at small negative fields ( $B_{\text{pc}} = -0.035$  T at  $T = 3$  K). With increasing temperature, the peak position  $B_{\text{pc}}$  moves towards zero. Above  $T = 10$  K, the hysteresis loops develop a minimum, which indicates the onset of the fishtail behaviour. This minimum shifts towards zero-field with increasing temperature.

Magnetization measurements on sample B at  $T = 4.2, 7, 10, 15, 20, 25, 30,$  and  $40$  K are presented in Fig. 2. Above  $T = 25$  K, the development of the fishtail shape is clearly visible. This graph demonstrates that at low temperatures the central peak is a dominant feature of the magnetization loop in the field range of a few tesla. Both the height and width of the central peak rapidly decrease with increasing  $T$ . At  $T = 4.2$  K, the position of the maximum,  $B_{\text{pc}}$ ,

is found at  $-0.12$  T and moves towards zero with increasing temperature, but stays negative up to  $T \approx 60$  K.

In Fig. 3a, the descending branches of the MHLs of the much thicker single crystal C are shown for temperatures between 10 and 70 K. In this crystal, the central peak is shifted much further towards negative fields ( $B_{pc} = -0.55$  T at  $T = 10$  K) as compared to the previous samples. The peak position moves rapidly towards zero in the temperature range between 10 and 30 K; above 30 K the magnitude of  $B_{pc}(T)$  decreases more slowly; and finally  $B_{pc}$  falls to zero above 70 K (see also Fig. 6 below). Note the apparent inconsistency in the  $M(B_e)$  dependence observed between 50 and 60 K. This is a consequence of a change in the shape of the fishtail peak from a broad low maximum into a rather sharp and high one at higher temperatures.

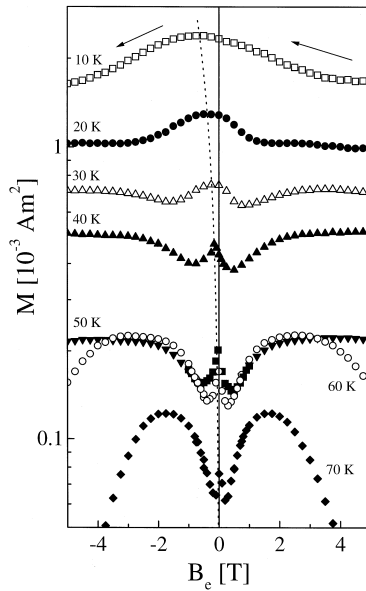


Fig. 3. The descending branches of the MHLs of sample C ( $d = 300 \mu\text{m}$ ) are shown for temperatures between 10 and 70 K. The central peak is shifted much further towards negative fields than in the previous samples ( $B_{pc} = -0.55$  T at  $T = 10$  K). From 40 K on, a higher field step density is used around 0 T. The dashed line indicates the temperature behaviour of the central peak. Note the apparent inconsistency in the  $M(B_e)$  dependence observed between 50 and 60 K which is caused by a very pronounced fishtail effect. The arrows indicate the direction of the field sweep.

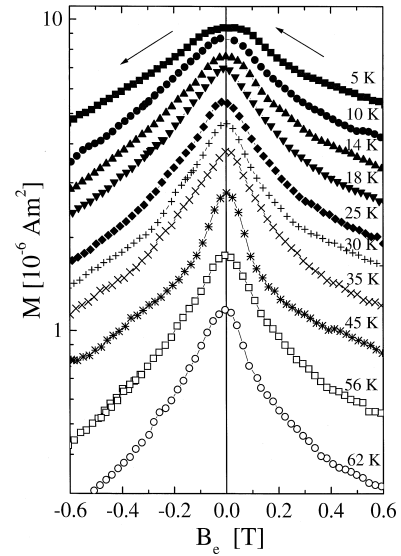


Fig. 4. Development of the central peak with temperature in an YBCO thin film measured by means of a VSM. Even at the lowest temperature measured the peak sits at zero external field. The dashed line indicates the temperature behaviour of the central peak; the arrows indicate the direction of the field sweep.

Fig. 4 presents the development of the central peak with temperature in the YBCO thin film measured by means of our VSM magnetometer. Even at the lowest temperature measured the peak sits at zero external field. The peak is much narrower as compared to the single crystals but also reduces with increasing temperature in a similar way to the behaviour in the single crystals shown previously.

Descending branches of magnetization loops measured by means of VSM on the Ag-sheathed Bi-2223 tapes and on the model sample are presented in Fig. 5a–c at temperatures between 3.4 and 70 K. The central peaks of all samples show an entirely different behaviour as compared to the other samples studied. In Fig. 5a, it is clearly visible that *the central peak is found for all investigated temperatures at positive fields on the descending field branch*. The positive position of the central peak becomes more and more pronounced with decreasing temperature as indicated by a dashed line. At  $T = 3.4$  K,  $B_{pc}$  of the monofilamentary tape is even as large as  $+0.17$  T [21]. The multifilamentary tape (Fig. 5b) and the model sample (Fig. 5c) also exhibit  $B_{pc}$  always at *positive* fields, but less pronounced.

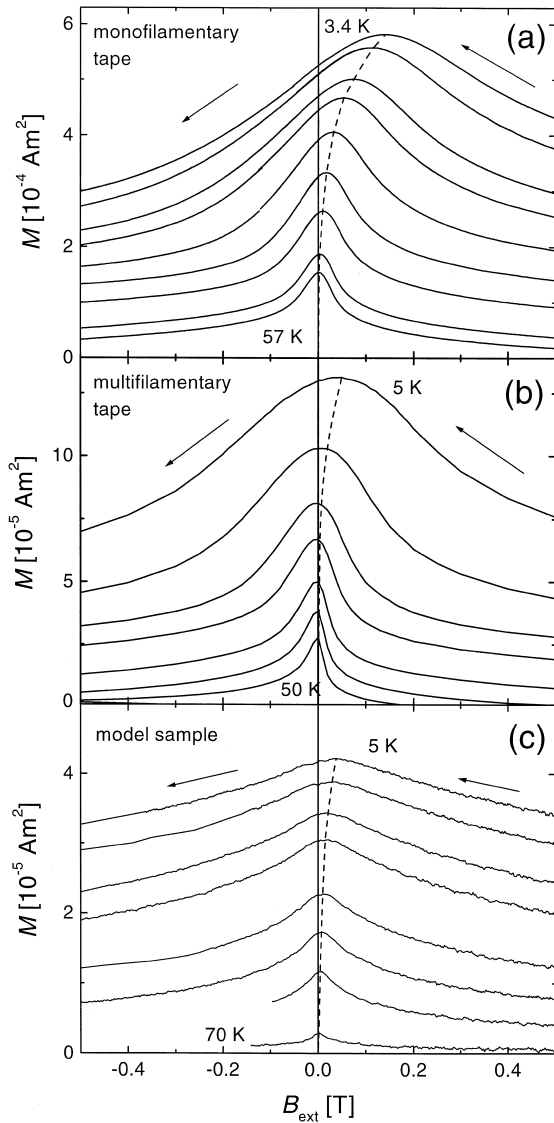


Fig. 5. Magnetic hysteresis loops measured on the Bi-2223 tapes and the model sample. The anomalous position of the central peak is indicated by a dashed line; the arrows indicate the direction of the field sweep. (a) MHLs of the monofilamentary tape at various temperatures 3.4 (outer loop), 6.2, 9.5, 11.8, 17.7, 26.2, 35.5, 49, and 57 K (inner loop). (b) MHLs of the tape with 19 filaments at temperatures between 5 (outer loop) and 50 K (inner loop). (c) MHLs of the model sample between 5 (outer loop) and 70 K (inner loop).

In Fig. 6, we plot the positions of the central peaks as a function of temperature for all samples investigated here. The effect of thickness (or aspect

ratio) on the position of the central peak is clearly visible: The central peak of the crystalline samples A to C is located at different negative fields according to their thickness. Sample C shows the peak at  $B_{pc} = -0.55$  T ( $T = 10$  K), sample B at  $B_{pc} = -0.12$  T ( $T = 4.2$  K), and sample A at  $B_{pc} = -0.035$  T ( $T = 3$  K). In contrast to the single crystals, the thin film exhibits the central maximum at zero-field for all investigated temperatures. The peak position of the Bi-2223 tapes anomalously occurs at positive fields; but the peak position of the multifilamentary tape is clearly less pronounced. In both tapes, the peak positions shift on decreasing temperature towards more positive values. The model sample is indeed capable of reproducing the anomalous peak position at positive fields. In contrast to the ‘real’ tapes, the peak is found always at lower positive fields. Furthermore, the temperature shift of the peak position is by far less pronounced here. For all samples, the peak has the tendency to shift towards zero with increasing temperature; the shift being more pronounced at low temperatures up to 30 K.

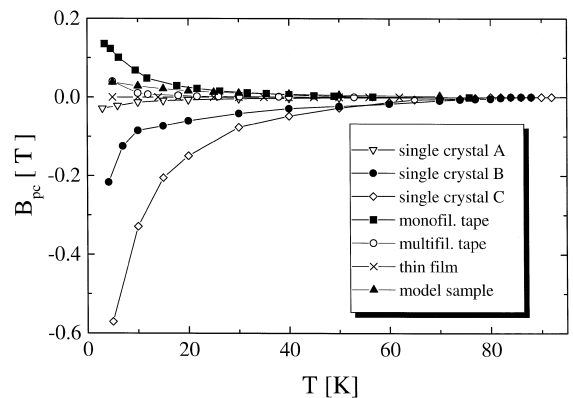


Fig. 6. The positions of the central peaks as a function of temperature for all samples investigated here; the lines are guide-lines for the eye. Sample C shows the peak at  $B_{pc} = -0.55$  T ( $T = 10$  K), sample B at  $B_{pc} = -0.12$  T ( $T = 4.2$  K), and sample A at  $B_{pc} = -0.035$  T ( $T = 3$  K). The YBCO thin film exhibits the central maximum at zero-field for all investigated temperatures. The peak position of the Bi-2223 tape anomalously occurs at positive fields, even as high as  $+0.17$  T at  $T = 3.4$  K. In all cases, the peak has the tendency to shift towards zero on increasing temperature; the shift being more pronounced at low temperatures up to 30 K. Above 60 K, the central peak has been observed at zero-field for all investigated samples.

Above 70 K, the central peak has been observed at zero-field for all investigated samples.

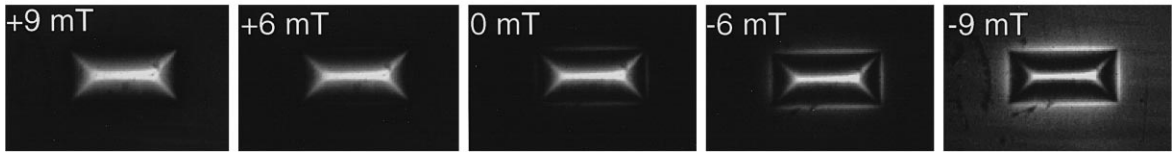
### 3.2. MO measurements of flux distributions around 0 T

Space-resolved flux distributions of three different samples were obtained by means of MO imaging in low magnetic fields around 0 T. As examples of homogeneous single crystalline samples we have chosen a YBCO thin film patterned into a rectangular shape and a thick, nearly cubic YBCO single crystal (sample D). In order to achieve maximum contrast, the MO investigations were performed at  $T = 18$  K unless noted otherwise. The polarizer/analyzer setting is chosen so that vortices of any

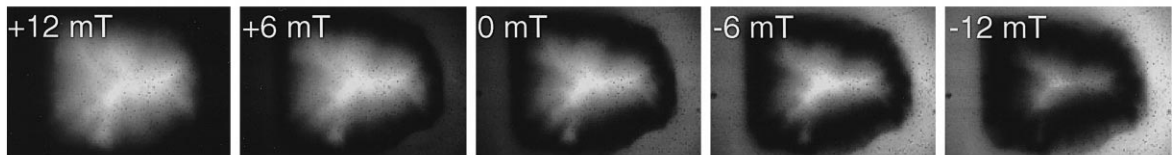
polarity will have the same intensity (see, e.g., Refs. [37–39] for a discussion). All samples were cooled in zero magnetic field, and subsequently the maximum field of +120 mT was applied. The images are then recorded in *decreasing* external field.

The upper row of Fig. 7 presents the flux patterns of the rectangular thin film at fields of +9, +6, 0, -6 and -9 mT (from left to right). Let us first discuss some general properties of the flux patterns in extreme perpendicular geometry. The rectangular YBCO thin film exhibits ideal, undisturbed flux patterns allowing a direct comparison with theoretically calculated flux profiles [40]. The basic features of the perpendicular geometry can be best described by regarding the remanent state (center image) first.

#### YBCO thin film



#### YBCO single crystal



#### Bi-2223 monofilamentary tape

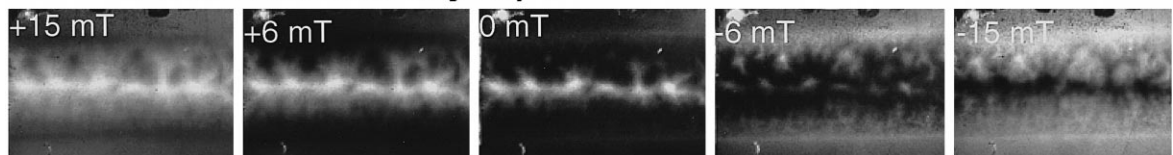


Fig. 7. MO flux patterns of three different high- $T_c$  samples; the sample dimensions are given in the text. The upper row presents flux patterns of the rectangular YBCO thin film at fields of +9, +6, 0, -6 and -9 mT (from left to right). The observation temperature is  $T = 18$  K. Note the presence of vortices of opposite polarity already at +6 mT. In the remanent state, the  $d$  line pattern is observed which is characteristic for a homogeneous sample in perpendicular geometry. The middle row presents the flux patterns of sample D at  $T = 77$  K, which had a nearly cubic shape ( $r_0/d \approx 1$ ). The field values are (from left to right): +12, +6, 0, -6 and -12 mT. The slightly irregular shape of the YBCO single crystal leads to a disturbance of the ideal flux pattern, but here the  $d$  lines of the currents are nearly washed away. Vortices of opposite polarity start to invade the sample only at a relatively high negative applied field. The lower row shows flux patterns of the Bi-2223 tape at  $T = 18$  K. The field values are (from left to right): +15, +6, 0, -6 and -15 mT. The flux distributions of the tape are complicated due to effects of granularity. Note that the tapes exhibit properties of homogeneous samples in perpendicular geometry like the  $d$  lines. However, due to the existence of some weak channels around some well-shielded grains, the behaviour of flux entrance and exit is irregular. The images of +15 and -15 mT are practically inverse to each other, i.e., the black and white regions are exchanged.

A characteristic, double-Y-shaped arrangement of lines dominates the flux pattern in the thin film. These lines, called discontinuity ( $d^+$ ) lines of the currents, are formed where the currents flowing parallel to the sample edges are forced to make a sharp turn [41,42]. During increasing field (see, e.g., Refs. [27,42]), these lines stay dark; in the remanent state, the  $d^+$  lines are bright. A detailed discussion of the features of the discontinuity lines, which are important to describe the current flow in superconductors, can be found in Refs. [41,42]. Another type of  $d$  lines, the  $d^-$  lines, are located along the sample circumference. In perpendicular geometry, both types of  $d$  lines are very pronounced as a direct consequence of the large demagnetization factors. During field increase, the  $d^-$  lines are very bright (“field overshoot”) as  $B_i > B_c$ . In the remanent state, the  $d^-$  lines are also represented bright. Now, let us discuss the effect of decreasing  $B_c$ . Starting from a fully penetrated state as in this experiment, the  $d^-$  lines become first dark as a consequence of the change in current flow. On further decrease of the field (see the image taken at +6 mT), a bright rim appears outside the sample in still positive fields. This bright rim is due to the fact that the field lines of the pinned vortices are forming closed loops, and thus the field direction is *opposite* to the applied field. These field lines then generate vortices of opposite polarity which eventually enter the sample when still  $B_c > 0$  holds. These vortices are separated from the remaining pinned ones by a dark zone, where a line with  $B_i = 0$  can be found. This line, called “annihilation zone” moves further inside the sample in decreasing field. The appearance of this annihilation zone at  $B_c > 0$  is characteristic for the extreme perpendicular geometry and a direct manifestation of the large demagnetization factor. All these effects can be well described using the newly developed models for perpendicular geometry [42–44], especially when the field dependence of  $j_c$  is taken into account [45]. On applying a negative field to the remanent state (right side) more and more negative vortices enter the sample. However, as the current density in the thin film sample is relatively large, a quite large negative field is necessary to remove all remaining positive vortices from the sample. For the present sample, this field is as large as 150 mT at  $T = 18$  K.

The middle row of Fig. 7 presents the flux patterns of sample D of nearly cubic shape ( $r_0/d \approx 1$ ). In order to reach a fully penetrated state also for this thick sample within our field limits, the observation temperature had to be increased to  $T = 77$  K. The field values are (from left to right): +12, +6, 0, –6 and –12 mT. The slightly irregular shape of the YBCO single crystal leads to a disturbance of the ideal flux pattern, but here the  $d$  lines of the currents are nearly washed away. Characteristic for the thick sample in the remanent state are the dark sample edges. A bright rim along the  $d^-$  lines, i.e., vortices of opposite polarity, are found to invade the sample only at a *relatively high negative applied field*. This directly implies that the annihilation process between positive and negative vortices can only start when also an external negative field is applied. The state with a minimum vortex density (i.e.,  $\langle B_i \rangle_m = 0$ ) is, therefore, only reached when  $B_c < 0$ . This is a direct indication that the central peak in the MHL is located at a small, but *negative* applied field.

In the lower row of Fig. 7, flux patterns of the monofilamentary Bi-2223 tape are shown, observed at  $T = 18$  K. The field values are (from left to right): +15, +6, 0, –6 and –15 mT. The flux distributions at this relatively low temperature are complicated due to effects of granularity as discussed in Ref. [35]. A detailed discussion of such flux patterns of Bi-2223 tapes can be found in Refs. [22,30,31,35,46,47]. Here, it is particularly important to note that the tapes exhibit properties of homogeneous samples in perpendicular geometry like the  $d^+$  and  $d^-$  lines as well as features of granular samples. Due to the existence of weak channels around some well-shielded grains, the behaviour of flux entrance and exit is irregular and the flux patterns as well as the  $d^+$  lines are strongly inhomogeneous throughout the sample. Negative vortices appear in the sample after field reduction to very low fields and the annihilation of the pinned flux takes place relatively “fast”, i.e., in a narrow range of  $B_c$ , in the present case  $\pm 15$  mT. All this causes the images of +15 and –15 mT to appear practically as inverse images, i.e., the black and white regions are exchanged with each other.

In order to study the influence of structural defects on the flux patterns, we present in Fig. 8a a remanent state of a YBCO thin film at  $T = 18$  K,

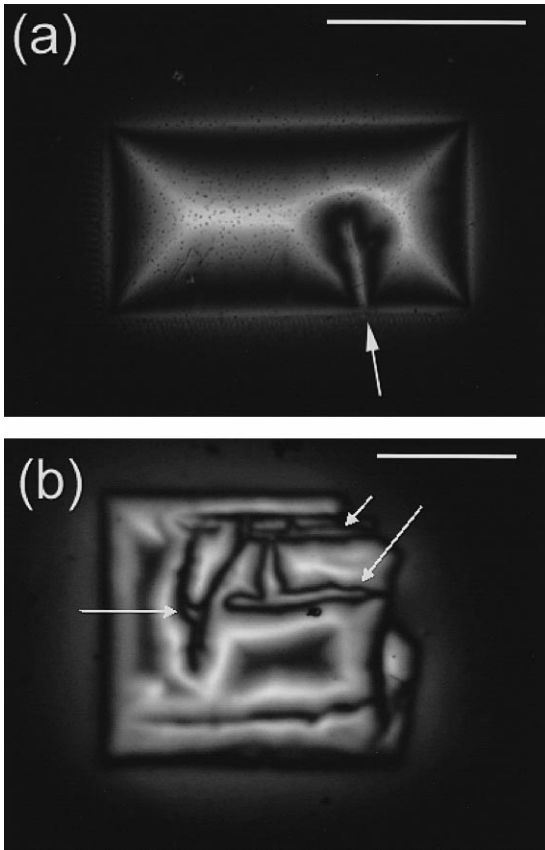


Fig. 8. (a) Remanent state of a YBCO thin film at  $T = 18$  K, which contains one large extended defect; the sample is similar to the film of Fig. 7. The marker is 1 mm long. The field distribution is obtained after zero-field cooling, applying a field of +120 mT and reducing it to 0 T. The arrow points to the defect line. Due to the large demagnetization factor of this thin film sample, the defect line acts as channel for easy flux penetration and exit. Consequently, the pattern of  $d$  lines is altered as compared to Fig. 7. (b) Flux pattern of the remanent state of sample E ( $T = 18$  K,  $B_e = 300$  mT, and reduced to 0 T); the marker is 1 mm long. The flux pattern is completely irregular, thus, causing the annihilation process to start at larger fields as for a homogeneous sample of the same shape. The arrows point to areas already penetrated by vortices of opposite polarity.

which contains one extended defect. This sample stems from the same batch as the film presented in Fig. 7. The image is obtained after zero-field cooling, then a field of +120 mT is applied and subsequently reduced to 0 T. Due to the large demagnetization factor of this thin film sample, the defect line acts as channel for easy flux penetration. Following

the classification of defects given in Ref. [48], also twin boundaries or dislocations in RBCO samples can act as such channels for easy flux penetration [37–39]. Such a situation is illustrated in Fig. 8b. This crystal (sample E) was detwinned by applying uniaxial stress parallel to the plate at  $T = 450^\circ\text{C}$ . However, structural defects (i.e., cracks in conjunction with a dislocation network) were introduced during this procedure. As a result, the flux pattern of the remanent state is completely distorted: In decreasing external field, vortices leave the sample along the defect lines, and, at still positive applied fields, negative vortices become stable along the defect line, thus, the annihilation process can start at much larger fields as compared to a completely homogeneous sample. In the remanent state, the  $d$  line pattern is distorted or, if a large number of such defects is present in the sample, even entirely vanished. In this way, a *thin* sample with a high density of structural defects may exhibit the central peak of the MHL also at slightly positive fields. With increasing thickness, the influence of defects on the remagnetization process becomes less important due

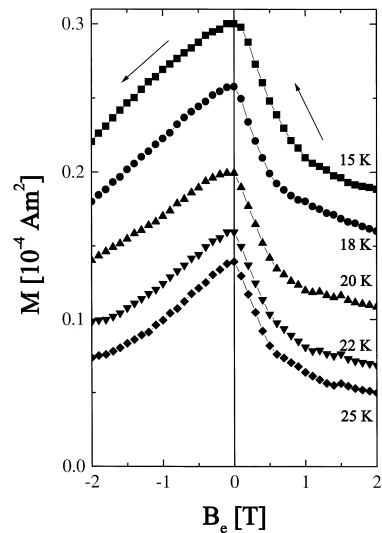


Fig. 9. MHLs of sample E at temperatures of 15, 18, 20, 22, and 25 K for comparison with the MO data. The peak position is found very close to 0 T, despite of the considerable extension in  $c$ -direction. Further, the shape of the central peak is clearly asymmetric; even after background subtraction. The arrows indicate the direction of the field sweep.

to the reduction of stray fields. To illustrate this, we present in Fig. 9 magnetization curves obtained on sample E. Despite its relative thickness, the peak position is found at around 0 T. One fingerprint of the influence of the defects can, however, be directly observed: The shape of the central peak is distorted, i.e.,  $dM/dB$  at positive fields is larger than at negative fields after passing 0 T. This was also observed in MHLs of a heavily twinned YBCO single crystal [49].

#### 4. Discussion

Samples of high- $T_c$  superconductors are mostly in the form of thin films and thin platelets (e.g., single crystals); so the demagnetization factor is large and the perpendicular geometry applies here. The silver-sheathed tapes of Bi-2223 or Bi-2212 have a geometry quite close to that of thin strips; so also these samples must be treated using the models of perpendicular geometry. Here, it is important to point out that bulk, melt-processed high- $T_c$  superconductors, where single-crystalline disk-shaped samples with diameters up to 10 cm and thicknesses up to 3 cm are grown, also have large demagnetization factors so that field overshoot effects along the sample edges are considerable. However, the thickness of these samples is fairly larger than  $\lambda$ , thus, these samples are forming a special class.

There is an important difference of the perpendicular geometry to the “classical” longitudinal geometry [24]: Induced, currents flow around the entire sample in all applied fields and consequently, large induced magnetic moments are observed. At low external fields, the generation of rather high stray fields is required to satisfy the boundary conditions and the corresponding flux distributions become complicated. The MO of flux distributions have shown that remanent state of a *thin* superconductor in the perpendicular geometry consists of pinned (trapped) flux lines in the sample centre and a thin rim of flux lines of opposite polarity along the edges (see, e.g., Fig. 7, upper row). The appearance of negative flux lines already *during* reduction of the external field from large positive values to 0 T is a pure demagnetization effect. Large self-fields gener-

ate negative (i.e., with opposite sign compared to the majority of the sample) flux lines in the regions close to the sample circumference. In thin samples, this happens already at rather large positive applied fields when sweeping the field towards zero. A similar effect was also already observed in thin Nb<sub>3</sub>Sn diffusion layers [50]. The sign change of the external field is accompanied by the entrance of flux lines of opposite polarity into the sample and by the formation of a front of zero  $B_i$  (“annihilation zone”) that propagates from the circumference towards the sample centre. The local induced supercurrents are obviously largest just at this front. Finally, as the external field approaches the value of full penetration, the zero-field front disappears at the sample centre. Above this value, all vortices within the (perfect) sample have the same polarity. With increasing sample thickness, this effect disappears and a remanent state with no negative vortices is observed, with  $B_i \approx 0$  along the sample edges.

Recently, models to calculate flux density profiles [42–45] and magnetization loops [51–53] were developed also for the perpendicular geometry. As in longitudinal geometry, magnetization loops calculated for the perpendicular configuration with a field-independent  $j_c$  do not show a central peak. Allowing a field dependent current [42,45] leads to an appearance of the central peak. This clearly demonstrates that the field dependence of  $j_c$  is essential for the observation of the central peak in a MHL. Recently, we could demonstrate in Ref. [26] that the peak position  $B_{pc}$  is located *strictly* at zero-field, i.e.,

$$\frac{\partial M}{\partial B_a} = 0 \text{ at } B_a = 0, \quad (1)$$

holds for *any* field dependence of the critical currents,  $j_c(B)$ . One additional effect is then sufficient to bring the peak towards the positive side. Such an additional effect may be granularity or a complicated sample shape, but could also be provided by structural defects. For the silver-sheathed tapes, the influence of granularity is the most important effect to be considered. Due to granularity, there are two contributions to the critical current; the intragranular and intergranular currents. Each of these two currents has

a different temperature behaviour: At low temperatures, the intragranular currents are larger than the intergranular ones and the sample behaves granular (e.g., some well-shielded grains can be seen within the flux patterns, thus, causing the ‘rough-looking’ flux patterns shown in Fig. 7, taken at  $T = 18$  K). However, also some indications of homogeneous samples like the  $d$  lines are present. In Ref. [35], it was shown that this granularity vanishes if the temperature is above 50 K, where the magnitude of the two contributions to the overall current are approximately equal. This process leads to the strange observation that the samples behave more granular at low temperatures. This vanishing of granularity with increasing  $T$  also restores the peak position, so that  $B_{pc} \approx 0$  T for  $T > 60$  K, see Fig. 6.

Tapes of Bi-2223 may exhibit the central peak of a MHL at positive fields in decreasing external field. Recently, models were developed to explain the anomalous position of the central peak in thin tapes [18,19,21]. Grains in the tapes are modelled by disks which are touching each other at the circumference. The idea of the modelling is that the actual internal field at the circumference of a flat grain is of opposite sign as compared to the low external magnetic field [54]. It is reasonable to expect that the currents at the disk circumference, which are contributing the largest portion to the total magnetic moment, reach the maximum value just when the internal field there becomes minimal. This happens when the external field cancels the axial component of the stray field of the grains  $B_{sz}$ , i.e., for  $B_e \approx -B_{sz}(r_0)$ . However, when the local field  $B_{iz}(r_0) \approx 0$ , the local field deep inside the grain is still non-zero. The next layer of grains therefore only slightly modifies this behaviour. Here, it is particularly important that the inter- and intragranular currents are comparable in magnitude. This is in stark contrast to granular YBCO, where the intragranular currents are several orders of magnitude larger than the intergranular currents [55]. The granularity, therefore, induces demagnetization fields which strongly modify the intergranular currents via their  $B$  dependence.

As the influence of granularity increases on decreasing temperature [35] due to the steep increase of the intragranular current density at low temperatures [35,56]. At elevated temperatures, the bulk pinning within the grains diminishes considerably so that the

intra- and intergranular current densities are approximately equal. Consequently, the peak position moves towards 0 T with increasing temperatures. In multifilamentary tapes, the grain growth and orientation along the silver sheath is better than for a monofilamentary tape. Therefore, the influence of granularity is not so important here and hence, the anomalous peak position is less pronounced. The model sample, which is a direct realization of one layer of disks, does indeed show the features predicted in the model calculations (see Fig. 5), as also in this case the central peak position is clearly anomalous, whereas an homogeneous film of the same type behaves ‘‘normally’’. Also the peak position shifts towards more positive fields on decreasing the temperature. The very steep increase found in a monofilamentary Bi-2223 is due to the steep increase of the intragranular current density, which cannot be modelled by means of a YBCO thin film.

In thin single crystals or thin films, the presence of structural defects is the most important factor for an anomalous behaviour of  $B_{pc}$ . Again, the large demagnetization factors enhance the influence of such defects (cracks with dislocation network, intergrowths, twin boundaries) considerably. It must, however, be noted that the accompanying distortion (see Fig. 9) of the central peak shape gives a clear indication of the presence of such defects.

Finally, it is worth to mention that the central peak in a magnetization loop plays a dominating role especially at low temperatures. Measurements of MHLs in RBCO samples revealed [7,57] that the central peak of a MHL interferes with the fishtail peak; the same holds for the secondary peak found in Bi-2212 single crystals [58]. At low temperatures, additional peak effects may only be seen as irregularities of the central peak shape. This situation gradually changes with increasing temperature: When the low-field peak becomes sufficiently slender and/or small, modifications of the MHL shape resulting from other effects can be observed. Especially interesting in this context is the observation of an intermediate peak between the central and the fishtail peak [8–10]. The origin of this peak was identified recently as the onset of pinning provided by the twin structure [10]. Despite that twin boundaries are commonly observed in single crystals of RBCO materials, the intermediate peak is only observed in some

YBCO and NdBCO single crystals, where the fishtail peak is located at very large fields. In all other samples either the central peak or the fishtail peak will entirely mask the intermediate peak.

## 5. Conclusions

The measurements and model considerations presented in this paper support the following conclusions.

(1) For most high- $T_c$  samples, the perpendicular geometry does apply. Calculations of field profiles and magnetization loops are only possible since very recently. However, the central peak can be fully explained within the framework of these models allowing a proper field-dependence of  $j_c$ . The steeper this dependence, the more pronounced the central peak. In samples with an aspect ratio close to 1, the peak is always located at small negative fields.

(2) The MO flux patterns clearly reveal the differences between thin and bulk samples. In thin samples, the flux at the sample circumference reverses already at positive applied fields and consequently, the central peak is located close to  $B_c = 0$  T at very low negative fields. With increasing sample thickness, the flux reverses at lower positive applied fields and finally, the sign reversal will take place together with the polarity of the external field. Correspondingly, the condition  $\langle B_i \rangle = 0$  takes place at higher negative fields and the central peak shifts to higher negative fields as well.

(3) Structural defects within the sample may alter the flux distributions considerably and facilitate the entry of vortices of opposite polarity. In defect-containing thin samples, the central peak may be observed even at slightly positive fields. A similar effect may occur in single crystals of poor quality or in crystals with an irregular shape.

(4) With increasing temperature, the central peaks of all samples are found to shift towards zero-field. This shift is connected with the decrease of pinning efficiency caused by thermal excitation, with the corresponding reduction of  $j_c$  and with demagnetization effects. Despite of the differences in the  $j_c(B_i, T)$  of individual samples, a common feature of all samples seems to be that the peak is found close to 0 T at temperatures above 60 K.

(5) Ag-sheathed Bi-2223 tapes are unique systems with a rest of granularity, where the inter- and intragranular currents give a comparable contribution to the magnetic moment. This interplay of currents is responsible for the formation of the central peak at small positive fields on the descending field branch. The MO images have clearly shown that the tapes cannot be treated as a homogeneous superconductor at low temperatures  $< 30$  K. By means of a model sample with artificially introduced granularity, the anomalous peak position of the tapes can be successfully reproduced; thus, underlining the importance of granularity.

(6) At low temperatures where the central peak dominates the MHLs at low fields, it may interfere with the observation of other peak effects within the magnetization loops. Only if the central maximum becomes sufficiently slender or narrow, other peaks may be observed.

In conclusion, we arrive at a following general scenario concerning the central peak position as theoretically demonstrated in Ref. [26]. Extended samples in parallel magnetic field show in their MHLs a central peak at a negative  $B_c$ , i.e., after passing through the remanent state on the descending field branch. As the sample thickness decreases, the peak position is shifted towards zero. In the limiting case of a uniform strip of infinitesimal thickness, it is located exactly at  $B_{pc} = 0$ . Granularity and/or structural defects lead to a shift of  $B_{pc}$  in the positive direction on the descending field branch. Thus, for a granular thin strip the peak is located at a *positive* field, i.e., before the remanent state is reached. The origin of this effect is that granularity induces demagnetization fields which strongly modify the intergranular currents via their  $B$  dependence.

## Acknowledgements

We would like to thank Y. Shen and P. Vase (NST, Brøndby, Denmark) for the excellent YBCO thin films and the Bi-2223 tapes; B. Nilsson and T. Claeson (Chalmers University, Göteborg, Sweden) for the preparation of the model sample. We acknowledge valuable discussions with Prof. M. Murakami (SRL/ISTEC, Div. 3, Tokyo), D.V. Shantsev (on leave from Ioffe Institute, St. Petersburg,

Russia) and Yu.A. Galperin (University of Oslo). The work carried out in Prague is supported by grant numbers A1010512/A1010919 of GA ASCR; the work at the University of Oslo is supported by The Research Council of Norway.

## References

- [1] L. Krusin-Elbaum, L. Civale, V.M. Vinokur, F. Holtzberg, *Phys. Rev. Lett.* 69 (1992) 2280.
- [2] K.A. Delin, T.P. Orlando, E.J. McNiff Jr., S. Foner, R.B. van Dover, L.F. Schneemeyer, J.V. Waszczak, *Phys. Rev. B* 46 (1992) 11092.
- [3] L.F. Cohen, J.R. Lavery, G.K. Perkins, A.D. Caplin, W. Assmus, *Cryogenics* 33 (1993) 352.
- [4] Y. Yeshurun, N. Bontemps, L. Burlachkov, A. Kapitulnik, *Phys. Rev. B* 49 (1994) 1548.
- [5] M. Werner, F.M. Sauerzopf, H.W. Weber, B.W. Veal, F. Licci, K. Winzer, M.R. Koblischka, *Physica C* 235–240 (1994) 2833.
- [6] A. Erb, J.-Y. Genoud, F. Marti, M. Däumling, E. Walker, R. Flükiger, *J. Low Temp. Phys.* 105 (1996) 1023.
- [7] M. Jirsa, L. Püst, D. Dlouhý, M.R. Koblischka, *Phys. Rev. B* 55 (1997) 3276.
- [8] A.A. Zhukov, H. Küpfer, G. Perkins, L.F. Cohen, A.D. Caplin, S.A. Klostov, H. Claus, V.I. Voronkova, T. Wolf, H. Wühl, *Phys. Rev. B* 51 (1995) 12704.
- [9] M.R. Koblischka, A.J.J. van Dalen, T. Higuchi, K. Sawada, S.I. Yoo, M. Murakami, *Phys. Rev. B* 54 (1996) R6893.
- [10] M. Jirsa, M.R. Koblischka, M. Murakami, *Phys. Rev. B* 58 (1998) 14771.
- [11] J. Senoussi, *J. Phys. (Fr.)* 2 (1992) 1041.
- [12] S. Senoussi, S. Hammond, F. Mosbah, in: A. Narlikar (Ed.), *Studies of High Temperature Superconductors*, Vol. 14, Nova Science Publishers, Commack, NY, 1994, p. 107.
- [13] K.V. Bhagwat, P. Chaddah, *Physica C* 224 (1994) 155.
- [14] P. Chaddah, in: A. Narlikar (Ed.), *Studies of High Temperature Superconductors*, Vol. 14, Nova Science Publishers, Commack, NY, 1994, p. 245.
- [15] M. Däumling, E. Walker, R. Flükiger, *Phys. Rev. B* 50 (1994) 13024.
- [16] M. Däumling, W. Goldacker, *Z. Phys. B* 102 (1997) 331.
- [17] S.B. Roy, A.K. Pradhan, P. Chaddah, *Physica C* 250 (1995) 191.
- [18] K.-H. Müller, C. Andrikis, H.K. Liu, S.X. Dou, *Phys. Rev. B* 50 (1994) 10218.
- [19] K.-H. Müller, C. Andrikis, Y.C. Guo, *Phys. Rev. B* 55 (1997) 630.
- [20] M.R. Cimberle, C. Ferdeghini, R. Flükiger, E. Giannini, G. Grasso, D. Marré, M. Putti, A.S. Siri, *Physica C* 251 (1995) 61.
- [21] M.R. Koblischka, L. Püst, A. Galkin, P. Nalevka, *Appl. Phys. Lett.* 70 (1997) 514.
- [22] M.R. Koblischka, T.H. Johansen, H. Bratsberg, L. Püst, A. Galkin, P. Nalevka, M. Maryško, M. Jirsa, M.D. Bentzon, P. Bodin, P. Vase, T. Freltoft, *J. Appl. Phys.* 83 (1998) 3798.
- [23] M.R. Koblischka, R.J. Wijngaarden, *Supercond. Sci. Technol.* 8 (1995) 199.
- [24] H. Ullmaier, *Irreversible Properties of Type-II Superconductors*, Springer-Verlag, Berlin, 1975.
- [25] M. Murakami, in: M. Murakami (Ed.), *Melt-Processed High Temperature Superconductors*, World Scientific, Singapore, 1992.
- [26] D.V. Shantsev, M.R. Koblischka, Y. Galperin, T.H. Johansen, L. Püst, M. Jirsa, *Phys. Rev. Lett.* 82 (1999) 2947.
- [27] M.R. Koblischka, T.H. Johansen, H. Bratsberg, L. Püst, Y. Shen, P. Vase, *J. Phys. C* 9 (1997) 10909.
- [28] M.R. Koblischka, L. Püst, A. Galkin, P. Nalevka, T.H. Johansen, H. Bratsberg, B. Nilsson, T. Claeson, *Phys. Status Solidi A* 167 (1998) R1.
- [29] M.R. Koblischka, L. Püst, A. Galkin, P. Nalevka, T.H. Johansen, H. Bratsberg, B. Nilsson, T. Claeson, *Phys. Rev. B* 59 (1999) 12114.
- [30] M.R. Koblischka, T.H. Johansen, H. Bratsberg, *Supercond. Sci. Technol.* 10 (1997) 693.
- [31] M.R. Koblischka, T.H. Johansen, H. Bratsberg, P. Vase, *Supercond. Sci. Technol.* 11 (1998) 479.
- [32] V.G. Hadjiev, C. Thomsen, A. Erb, G. Müller-Vogt, M.R. Koblischka, M. Cardona, *Solid State Commun.* 80 (1991) 643.
- [33] P. Vase, Y. Shen, T. Freltoft, *Physica C* 180 (1991) 90.
- [34] P. Bodin, Z. Han, P. Vase, M.D. Bentzon, P. Skov-Hansen, R. Bruun, J. Goul, *IOP Conf. Ser.* 158 (1997) 1299.
- [35] M.R. Koblischka, T.H. Johansen, H. Bratsberg, P. Vase, *Supercond. Sci. Technol.* 12 (1999) 113.
- [36] T.H. Johansen, M. Baziljevich, H. Bratsberg, Y. Galperin, P.E. Lindelof, Y. Shen, P. Vase, *Phys. Rev. B* 54 (1996) 16264.
- [37] T. Schuster, M.R. Koblischka, N. Moser, H. Kronmüller, *Physica C* 179 (1991) 269.
- [38] T. Schuster, M.R. Koblischka, B. Ludescher, H. Kronmüller, *J. Appl. Phys.* 72 (1992) 1478.
- [39] T. Schuster, M.R. Koblischka, B. Ludescher, H. Kronmüller, *Z. Metallkd.* 83 (1992) 618.
- [40] M.R. Koblischka, T.H. Johansen, submitted for publication.
- [41] T. Schuster, M.V. Indenbom, M.R. Koblischka, H. Kuhn, H. Kronmüller, *Phys. Rev. B* 49 (1994) 3443.
- [42] T. Schuster, H. Kuhn, E.H. Brandt, M.V. Indenbom, M.R. Koblischka, M. Konczykowski, *Phys. Rev. B* 50 (1994) 16684.
- [43] E.H. Brandt, M.V. Indenbom, *Phys. Rev. B* 48 (1993) 12893.
- [44] E. Zeldov, J.R. Clem, M. McElfresh, M. Darwin, *Phys. Rev. B* 49 (1994) 9802.
- [45] J. McDonald, J.R. Clem, *Phys. Rev. B* 53 (1996) 8643.
- [46] A.E. Pashitski, A. Polyanskii, A. Gurevich, J.A. Parrell, D.C. Larbalestier, *Physica C* 246 (1995) 133.
- [47] A.E. Pashitski, A. Polyanskii, A. Gurevich, J.A. Parrell, D.C. Larbalestier, *Appl. Phys. Lett.* 67 (1995) 2720.
- [48] M.R. Koblischka, *Supercond. Sci. Technol.* 9 (1996) 271.
- [49] T. Tamegai, T. Shibauchi, S. Ooi, H. Nakagawa, T. Kumeno, *Advances in Superconductivity VII*, Springer-Verlag, Tokyo, 1994, p. 419.

- [50] R. Potratz, W. Klein, H.U. Habermeier, H. Kronmüller, *Phys. Status Solidi A* 60 (1980) 417.
- [51] E.H. Brandt, *Phys. Rev. B* 58 (1998) 6506.
- [52] E.H. Brandt, *Phys. Rev. B* 58 (1998) 6523.
- [53] T.B. Doyle, R. Labusch, R.A. Doyle, *Physica C* 290 (1997) 148.
- [54] M. Däumling, D.C. Larbalestier, *Phys. Rev. B* 40 (1989) 9350.
- [55] M.R. Koblischka, T. Schuster, H. Kronmüller, *Physica C* 219 (1994) 205.
- [56] M.R. Cimberle, C. Ferdeghini, G. Grasso, C. Rizzuto, A.S. Siri, R. Flükiger, F. Marti, *Supercond. Sci. Technol.* 11 (1998) 837.
- [57] M. Jirsa, L. Püst, *Physica C* 291 (1997) 17.
- [58] D.T. Fuchs, E. Zeldov, T. Tamegai, S. Ooi, M. Rappaport, H. Shtrikman, *Phys. Rev. Lett.* 80 (1998) 4971.